Journal of Engineering and Applied Sciences 13 (19): 7803-7808, 2018
ISSN: 1816-949X

Simple Experimental Model for Bond Stress and Slip Between HPFRCC and FRP Strip Used as a Permanent Form

Seung-Woon Yoo
Department of Civil Engineering, Catholic Kwandong University, 24, Beomil-ro, 579 Beon-gil, Gangneung-si, 25601 Gangwon-do, Korea

Abstract: Using a GFRP (Glass Fiber Reinforced Polymer) strip was used as a tensile bar and concrete form markedly reduces the construction period and construction costs. A local bond stress and slip model that is critical in the analysis and design of the concrete combined structures was suggested. Two types of FRP planks were utilized as permanent form and tensile reinforcement to perform a comparison test about the bond stress between the FRP and concrete. GF12 of RFCON was 2.00~2.50 MPa and GF22 was 2.80~5.10 MPa. For the simple model this study suggests in case of RFCON, the maximum mean local bond stress is 3.10 MPa, the initial gradient is 55.49 MPa/mm and the total slip is 0.28 mm. In this study, an experiment of flexural bonding failure were performed and results were analyzed to study the bonding and slip behavior between FRP strip and concrete. It was proposed a simple experimental model that can be easily applied to the composite concrete structures.

Key words: FRP strip, permanent form, high performance, concrete, bond stress, composite structure

INTRODUCTION

Recently, there have been numerous applications of fiber reinforced polymer composite materials for construction and other fields (Bank, 2006). One common example is the use FRP as internal reinforcement ('rebars') and external reinforcement of concrete structures. FRP reinforcing materials are generally used for reinforced concrete structures to prevent corrosion, a problem that plagues conventional reinforced and prestressed concrete structures. In addition, FRP materials have been widely used for repairing or strengthening damaged and corroded concrete structures (Bank *et al*., 2007). The use of hybrid FRP and concrete composite members with a dual purpose of concrete form and reinforcement has been considered in some research and construction cases (Deskovic *et al*., 1995; Hall and Mottram, 1998). A combined concrete form and tensile system can apply rapid construction of concrete structures because of there is no time consuming of assembly and dismantling of conventional reinforced concrete system.

The FRP plank-concrete composite member system has some differences from the more widely studied use of epoxy to bond FRP to the deteriorated and corroded structure as a means of repair and strengthening (Cheng *et al*., 2005). In this study an experiments of flexural bonding failure were performed and results were analyzed to study the bonding and slip behavior between FRP plank and concrete. It was proposed a simple experimental model that can be easily applied to the composite concrete structures.

Table 1: Fiber properties

Groups	Color	Class	Density	Length (mm)	Diameter (μm)	Tensile strength (MPa)	Elastic modulus (GPa)
RF4000	yellow	PVA	1.30	30	600	900	28
RSC15	white	PVA	1.30	8	40	1.300	37
RECS100L	white	PVA	1.30	12	100	1.100	25
RFS400	white	PVA	1.30	18	200	1.000	29
KLON1000	white	PVA	1.26	8	15	890	15
PP-macro	white	PP	0.91	48	0.5~1.0	450	5.6

Table 2: Compressive and tensile strength of the specimen

Concrete (DF)	Fiber type	Compressive strength (MPa)	Tensile strength strength (MPa)
1	NC	41.17	1.83
2	RF4000	35.00	2.65
3	RSC15	27.69	2.23
4	RSC15	31.65	2.44
5	PP	22.64	2.17
6	RF4000+RSC15	30.58	2.93
7	PP+RSC15	25.45	2.67
8	RECS100L	28.76	2.23
9	RFS400	25.65	1.86
10	KLON1000	30.46	1.97

Experiment outline and HPFRCC: For reinforcing fiber in concrete, RF4000, RSC15, RECS100L, RFS400, KLON1000 Polyvinyl Acetate (PVA) and Polypropylene (PP)-macro types were used (Yoo and Yoo, 2016). The physical properties of each fiber are summarized in Table 1 and data on the mix design table to measure tensile strength are presented in Table 2.

The compressive and tensile strength were tested. The maximum average compressive strength was 22.64~41.17 MPa and tensile strength was 1.86~2.93 MPa.

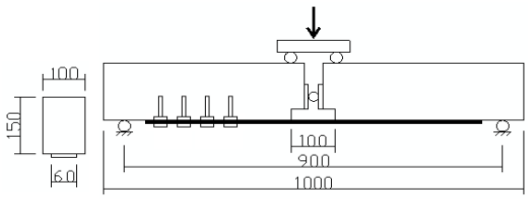

Fig. 1: Dimensions of test specimen(mm)

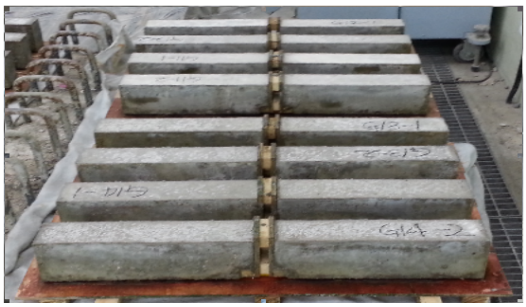

Fig. 2: Test specimens

Compressive strength did not increase for mixed fiber reinforcement. Among the mixtures of concrete and reinforcing fibers, DF2 of RF4000 specimens and DF5 of PP specimens displayed the highest and lowest compressive strength (35.00 and 22.64 MPa, respectively). The result for the PP fiber reflects the water insolubility of the fiber compared to other fibers. Tensile strength testing revealed the highest value (2.93 MPa) for the DF6 specimen. DF2 and 5 specimens had the best performance when the tensile strength was beyond its maximum. This may be due to the lengths of the reinforcing fibers in DF2 and 5 specimens which were the longest. The shorter the fiber, the lower was the performance (Fig. 1 and 2).

MATERIALS AND METHODS

Experimental outline and experimental specimens: In the experiment, RF4000 of PVA group, designated RFCON, was used as the reinforcing fiber. Compressive strength was 34.69~44.44 MPa and tensile strength was 2.03~3.26 MPa. The beam bending test that was used is thought to be as the best method to describe the bond behavior of FRP-concrete composite members.

The specimens used in this experiment were 1000 mm long and 100×150 mm. A detailed figure and measurements are presented in Fig. 1. There were four different independent cases and two specimens were made for each case for a total of eight. GFRP plank and HPFRCC was attached on only one side by epoxy bond.

The other side was fixed with a small anchor bolts. The mechanical properties of the epoxy and GFRP plank

Table 3: Properties of bond epoxy

Tensile strength (MPa)	Compressive strength (MPa)	Shear strength (MPa)	Elogation at break (%)
77.9	84.0	18.3	4.8

Table 4: Properties of GFRP

Groups	Class	Thickness (mm)	Tensile strength (MPa)	Elastic modulus (GPa)
GFRP1	Glass	8.0	395	19.9
GFRP2	Glass	5.0	514	33.6

Table 5: Classification of test specimens

Group/No.	Specimen	Type of FRP	Concrete
GF1			
1	GF11	GFRP1	RFCON
2	GF12	GFRP1	RFCON
GF2			
1	GF21	GFRP2	RFCON
2	GF22	GFRP2	RFCON

are detailed in Table 3 and 4 and the categorization details of the test specimen are provided in Table 5. The test specimens were produced as follows. First, the FRP plank was cut as a rectangle 60 mm wide and 800 mm long with no other manipulation other than dust cleaning. Sand was deposited to a depth of 4-7 mm on the GFRP plate by epoxy (S company, Swiss). Using this FRP plank as a cast, the specimens were created with cast-in-place high performance fiber Reinforced Cementitious Composites (RFCON).

Instrumentation and failure mode: All specimens were loaded at center of the span until a failure occurs. The failure occurred at the interface between GFRP strip and concrete as expected and there was no separation at the other side where steel anchor were fixed. The overall failure shape was well balanced in lateral direction and there was no local failure.

The data was acquired through an electric resistance strain gauge attached to the FRP plank, LVDT and a load cell. Ten electric strain gauges were set up. The first electric gauge, G0 was set up at the middle of the FRP plank where no concrete was attached. The spots where concrete was attached were the locations of G1. G2 through G6 were set up 15 mm apart from each other, G7 with a 30 mm separation, G8 with a 60 mm separation and G9 with a 90 mm separation. LVDTs were set up at the both sides of the setting, one on each to measure deflection at the position of G0. More detailed positions of strain gauges are shown in Fig. 3.

For the failure shape of RFCON, GFRP1 and GFRP2 mostly showed destruction between the FRP plank and epoxy accompanying destruction between FRP plank and the concrete with no significance apparent to the naked eye. No special separation by RFCON was observed but the microcrack on the spots without bond failure was dispersed widely in case of RFCON compared to normal concrete.

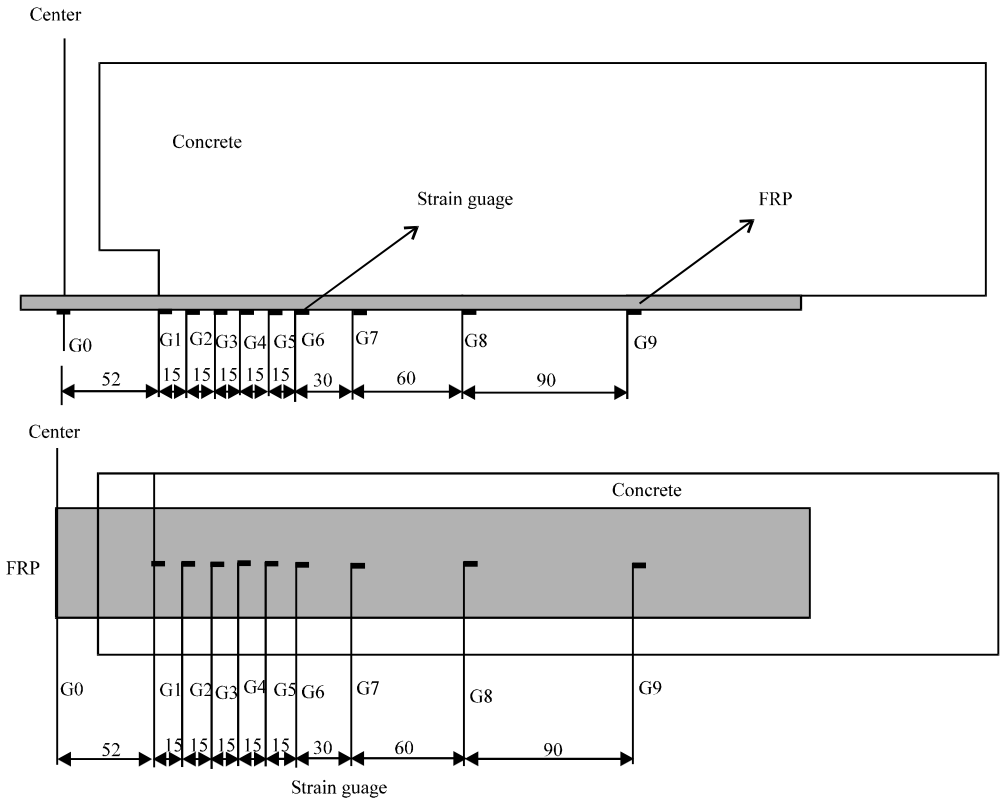

Fig. 3: Location of strain gauges on the test specimen

RESULTS AND DISCUSSION

Distribution of strain and local bond stress-slip relationships: There were three stages of strain distribution depending on the level of the applied load. At the initial stage of applied loading, the G1 gauge showed the largest strain and the strain decreased markedly moving to the end of the FRP strip. The strain distribution changed as hair cracks developed near the location where the G1 gauge was attached as the applied load was increased. The strain increased from the location where G1 gauge was attached to the end of the FRP strip and decreased linearly after reaching peak stress. The location with the peak value of strain distribution moved to end of the FRP strip as the applied load reached failure.

The local bond stress was obtained from the measured strains at each location. The local bond stress between two neighbouring strain gauges can be calculated from Eq. 1, since, the strains were measured with specified spacing in this study. The variation of shear stress in the longitudinal direction is determined (Nakaba *et al*., 2001; Dai *et al*., 2005):

$$\tau_{i,i+1} = tE\frac{\varepsilon_i - \varepsilon_{i+1}}{x_{i+1} - x_i}, i = n,3,2,1 \quad (1)$$

Where:

$\tau_{i, I+1}$ = The local bond stress between G_i and G_{i+1}

ε_i = The strain at location of G_i and x_i is value of x coordinate (Fig. 4 and 5)

The slip between two neighbouring strain gauges is calculated from Eq. 2, since, the strains were measured with specified spacing in this study:

$$S_{i,i+1} = S_{i+1,i+2} + (\varepsilon_i + \varepsilon_{i+1})\frac{x_{i+1} - x_i}{2}, i = n,3,2,1 \quad (2)$$

Where

$S_{i, I+1}$ = The slip between location i and I+1

ε_i = The strain at location of G_i, x_i is value of x coordinate

Pull-out force and interfacial fracture energy: The pull-out force applied to the FRP strip was calculated from the equilibrium equation and the strain gauge attached at the center of the FRP strip. The pull-out force calculated from the equilibrium was used, since, it shows a similar value compared to the force calculated from the strain gauge.

The bond stress occurs at the interface of the GFRP strip and concrete as the tensile force applies to the FRP

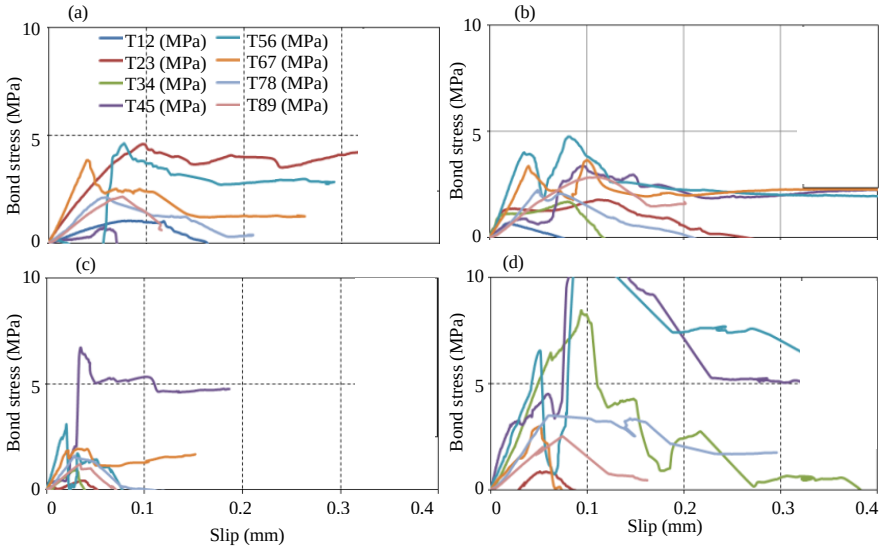

Fig. 4: Bond stress-slip relationship of GF1 and GF2

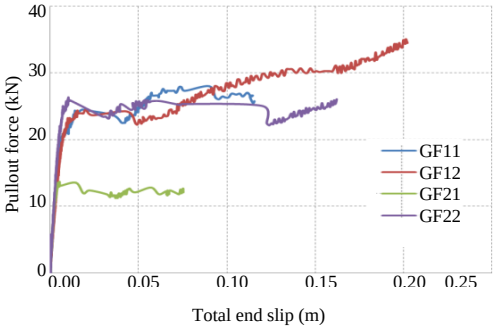

Fig. 5: Pull-out force-total end slip curve

strip. It is ideal relation that the bond stress first increase gradually at the location where bonding starts, the stress decrease as the micro crack occurs between FRP strip and concrete after reaching maximum bond stress, the maximum bond stress transfers to the adjacent region and finally the failure occurs at the entire bonding area.

The interfacial fracture energy which is obtained from the area below the bond stress-slip curve is a useful value to characterize the bond strength and failure mechanism of the bonded surface (Dai *et al*., 2005). The interfacial fracture energy is given by Eq. 3 (Taljsten, 1997):

$$G_f = \frac{P^2}{2Etb^2} \quad (3)$$

Where:

G_f = The interfacial fracture energy
P = The critical load applied to FRP strip
b = The width of FRP strip
t = The thickness of FRP strip
E = The modulus of elasticity

Suggestion of simple bond stress and slip model: The bond stress-slip curves at each section are depicted in Fig. 5. The curves tended to be widely dispersed at each section. This phenomenon is also evident as an attachment characteristic in old structures in which FRP is used as reinforcement epoxy. Excessive values were evident for the strain gauge at G1, the starting point, because of the sudden change of stress caused by the abrupt bending of the FRP. For strain gauges G7-G9, the back part of the attachment site between FRP plank and concrete was destroyed rapidly. The average local strain values from G2-6 gauges were used to analyze the local bond stress and slip characteristic between the FRP plank and concrete to get more reasonable data.

Generally, some simplified relationship of the local bond model was suggested in various forms. Among them, the double linear relationship model seemed to be the most simple and reasonable relationship. The present data support a simple local bond stress and slip model by calculatin g reasonable values of local stress, gradient and total slip amount based on the supplied equations (Fig. 6).

In the simple model curves, the overall shape was similar. However, the peak value of local bond stress and initial slope is reasonable but the parts after peak showed a little difference. Therefore, the simple bond and slip model suggested here treats the part before the bond stress reaches peak and the part after separately.

For the portions where the curves ascended, the experimental results were used because the bond stress relationship induced from the experiment was generally consistent. The average bond stress of peak and gradient of ascending part of experiments are provided in

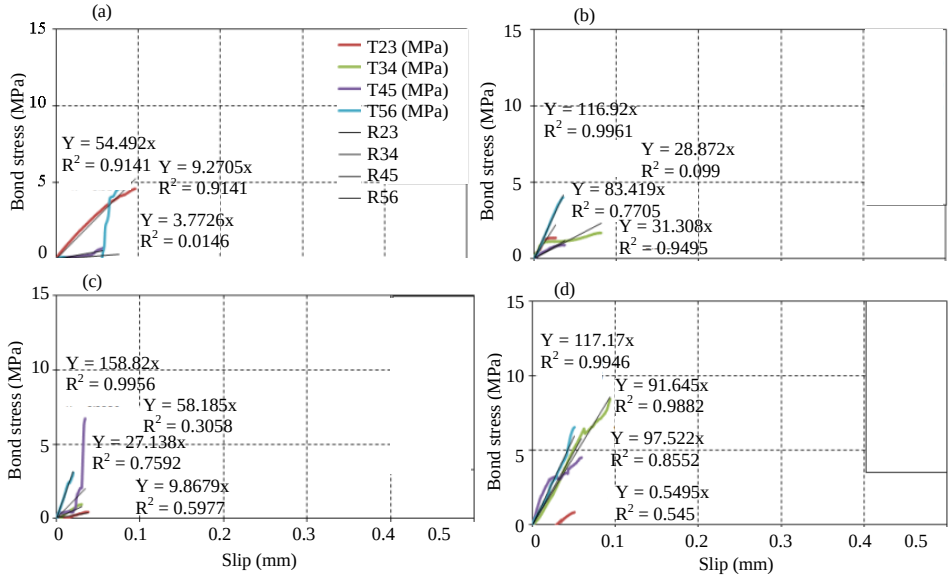

Fig. 6: Bond stress-slip curve of GF1 (1, 2), GF2 (1, 2)

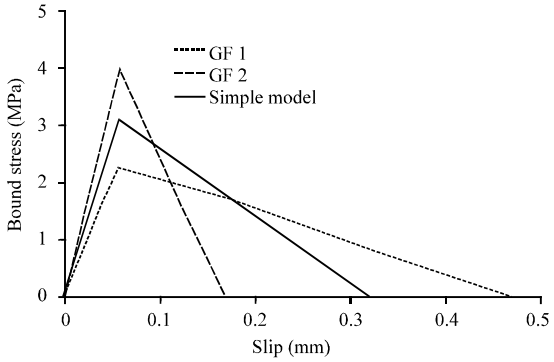

Fig. 7: Proposal of simple bond stress and slip model

Table 6: Mean bond stress between gauges (MPa)

	Bond stress				
Specimen (No.)	G_2, G_3	G_3, G_4	G_4, G_5	G_5, G_6	Mean bond stress
GF1					
1	4.60	0.02	0.74	4.63	2.52
2	1.37	1.70	0.90	4.02	2.00
GF2					
1	0.44	0.96	6.73	3.08	2.80
2	0.85	8.46	4.52	6.56	5.10

Table 7: Fracture energy (kN/m)

Specimen	GF11	GF12	GF21	GF22
Fracture energy	0.52	0.52	0.15	0.57

Table 6-8. The interfacial fracture energy concept was used instead of direct experimental stress and gradient because of the rest part of peak showed a trend in which the data became distributed. In other words, this portion in the model is the interfacial fracture and the value could be gained by using Eq. 3. This value is equivalent to the

Table 8: Initial gradient between gauges (MPa/mm)

	Initial gradient				
Specimen (No.)	G_2, G_3	G_3, G_4	G_4, G_5	G_5, G_6	Mean gradient
GF1					
1	54.49	0.00	3.77	9.27	16.88
2	83.42	31.31	28.87	116.92	65.13
GF2					
No. 1	9.87	27.14	58.19	158.82	63.51
No. 2	0.55	91.65	97.52	117.17	76.45

Table 9: Gradient and slip in rear part

Specimen (No.)	Gradient (MPa/mm)	Final slip S2 (mm)
GF1		
1	16.88	0.42
2	65.13	0.52
GF2		
1	63.51	0.11
2	76.45	0.22

area of bilinear curve, so that, the total slip length can also be determined. The data are provided in Table 9. The data are provided in Table 9 and Fig. 7 depicts the suggestions of the simple bond model.

CONCLUSION

Using a glass fiber reinforced polymer plank was utilized as a tensile reinforcing material and permanent form markedly reduces the construction period and construction costs. It was conducted experiments to estimate the bond and detach performance between cast-in-place high performance fiber reinforced cementitious composites and GFRP which was utilized as permanent form and main tensile reinforcement.

A local bond stress and slip model that is critical in the design of the FRRP and concrete composite was suggested. Two types of GFRP planks were utilized as permanent form and tensile reinforcement to perform a comparison test about the bond stress and slip between the GFRP and concrete. Depending on the GFRP type, GFRP1 generally showed breakdown shapes in which the destruction between the FRP plank and epoxy and between FRP and concrete were mixed. GFPR2 also showed a very similar result. GF1 of RFCON was 2.00~2.50 MPa and GF2 was 2.80~5.10 Mpa.

SUGGESTIONS

For the simple model this study suggests in case of RFCON, the maximum mean local bond stress is 3.10 MPa, the initial gradient is 55.49 MPa/mm and the total slip is 0.28 mm.

REFERENCES

Bank, L.C., 2006. Composites for Construction: Structural Design with FRP Materials. John Wiley & Sons, Hobokn, New Jersey, USA., ISBN-13:978-0471-68126-7, Pages: 552.

Bank, L.C., M.G. Oliva, H.U. Bae, J.W. Barker and S.W. Yoo, 2007. Pultruded FRP plank as formwork and reinforcement for concrete members. Adv. Struct. Eng., 10: 525-535.

Cheng, L., L. Zhao, V.M. Karbhari, G.A. Hegemier and F. Seible, 2005. Assessment of a steel-free fiber reinforced polymer-composite modular bridge system. J. Struct. Eng., 131: 498-506.

Dai, J., T. Ueda and Y. Sato, 2005. Development of the nonlinear bond stress-slip model of fiber reinforced plastics sheet-concrete interfaces with a simple method. J. Compos. Constr., 9: 52-62.

Deskovic, N., U. Meier and T.C. Triantafillou, 1995. Innovative design of FRP combined with concrete: Long-term behavior. J. Struct. Eng., 121: 1079-1089.

Hall, J.E. and J.T. Mottram, 1998. Combined FRP reinforcement and permanent formwork for concrete members. J. Compos. Constr., 2: 78-86.

Nakaba, K., T. Kanakubo, T. Furuta and H. Yoshizawa, 2001. Bond behavior between fiber-reinforced polymer laminates and concrete. Struct. J., 98: 359-367.

Taljsten, B., 1997. Defining anchor lengths of steel and CFRP plates bonded to concrete. Intl. J. Adhes. Adhes., 17: 319-327.

Yoo, S.W. and J.S. Yoo, 2016. Simple bond stress-slip experimental model between GFRP plate and cast-in-place HPFRCC. Adv. Sci. Technol. Lett., 124: 21-25.